Performance evaluation of bridgeless isolated SEPIC-Luo converter for EV battery charging using PI and ANN controller

Meena Dhandapani[1], Padmathilagam Ravichandran[1], Arulvizhi Shanmugam[2], Nammalvar Pachaivanan[3]

[1]Department of Electrical Engineering, Faculty of Engineering and Technology, Annamalai University, Chidambaram, India
[2]Department of Electrical and Electronics Engineering, CK College of Engineering, Cuddalore, India
[3]Department of Electrical and Electronics Engineering, Builders Engineering College, Nathakadaiyur, India

Article Info

ABSTRACT

Electric vehicle (EV) rechargeable battery packs that employ traditional power factor correction (PFC) circuit design have performance limitations due to their substantial conductivity loss that ensures at the input of a diode bridge rectifier (DBR). This study suggests a bridgeless (BL) isolated single ended primary inductance converter (SEPIC) - Luo converter to address the problem. As a result, the input current exhibits a power factor operation of unity throughout the charging process. DBR elimination and current conduction through a remarkably small number of circuits both significantly reduce conduction losses. The use of an artificial neural network (ANN) and proportional integral (PI) controller enhances the converter's performance with a stable DC link voltage. The suggested converter overall operation is thoroughly described in terms of variety of operating modes and simulation-based effectiveness. Here, with the assistance of the hysteresis current controller (HCC), the input current disruptions are reduced. Constant current and voltage management is used to successfully charge the EV battery, resulting in improved efficacy and inherent PFC. By utilizing simulation outcomes achieved from MATLAB, the performance of proposed BL isolated SEPIC-Luo in boosting the power quality of EV charger system is examined.
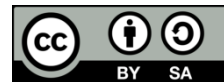
Corresponding Author:

Meena Dhandapani
Department of Electrical Engineering, Faculty of Engineering and Technology, Annamalai University
Chidambaram, Tamilnadu, India
Email: meenadhandapani86@gmail.com

1. INTRODUCTION

Electric vehicles are driven by employing battery packs to deliver the required amount of friction. In order to achieve efficient energy consumption as well as a further decrease in carbon dioxide emissions, the automotive sector is evolving towards electrical vehicles including cars and bikes. These alternatives have been developed to stabilize the transportation sector towards a green and sustainable aspect. The battery energy storage (BES) used in current and emerging vehicle technologies includes a recharging system that comprises specialized power electronic interfacing circuits [1]–[3]. Such power electronic device connections developed effectively have to preserve the required power quality (PQ), as it controls the charging voltage for BES [4], [5]. This work makes use of AC-DC conversion with power factor correction (PFC) to preserve the unity power factor and lower total harmonic distortion (THD). An essential component of an electric vehicle (EV) charger is front-end PF adjustment. The effectiveness and compactness of the PFC converter must be achieved, as well as has to adhere to global PQ rules. The incorporation of an extra PFC phase in a typical battery, which threatens the foregoing size and performance criteria because of the charger's larger size and higher price, is necessary

to deliver better PQ indices at AC mains. As a result, single stage PFC converters are the subject of substantial market analysis [6]. A review of different front end PFC converters for EV charging devices depending on the layout is presented in [7]. Relying on both the on- and off-board arrangements, an EV charger may be constructed. The articles [8] through [9], [10] explore several single stage EV chargers depending on on-board setups that have increased energy capacity and reliability. With the benefit of reducing the weight of the vehicle and the ability to charge at larger power ratings, an off-board design appears to be more attractive. For the off-board EV charger, a novel front end interleaved PFC converter has been proposed in [11] that also lowers the excessive current ripple caused by frequency. As a result, the filter's width is decreased, also the control devices are implemented simultaneously and the system's semiconductor deficits have been decreased. The problem of heat stress in the diode bridge rectifier (DBR) input terminal is not resolved by interleaving, in contrast to conventional boost rectifier. A variety of converters with interleaved input and PFC-based zero amplitude changing EV adapters are described in [12]–[14]. These converters have the intrinsic benefit of lower output current ripple and inductor size. An improved PQ-based converter cannot interleave inputs due to the drawback of higher electrical stress in PFC switches.

Power electronics systems' primary choice for providing an integrated PFC in unidirectional EV chargers has always been traditional DBR-driven boost converters. The performance of boost converters, however, degrades at high power levels due to increased inductor size and bridge losses and if a minimum amount of inductor is used, there is an increase in high frequency ripple in the DC-link capacitor. Both are still not advised for PFC in the charger due to the insufficient pattern capability and constrained duty cycle of the buck and boost converters. The ability to step up and down over a wider range of input voltages makes buck-boost converters [15] the most useful option for PFC in EV chargers. Thus, it is mandatory that EV applications require a particular converter topology for battery charging operations. The previous studies [16]–[18] discuss a thorough analysis of numerous single-phase AC-DC buck-boost PFC converters, including the state of the art, setups and functional testing in wide variety of applications. Nevertheless, input diode bridge topologies have become more energy inefficient and the device's harmonics stress raises as a result of the diode bridge. Many endeavors have been undertaken in the research to build bridgeless PFC converter topologies in order to achieve the highest power distribution efficiency. By removing the input DBR and minimizing the amount of semiconductor devices that the current must pass through, the switch conduction loss is lowered. Several isolated bridgeless converters based on Buck boost designs including SEPIC [19] [5] [20] Cuk [21] [22] zeta [23] and Luo [24] converters, have been proposed to address the aforementioned problems. For battery charging applications, the bridgeless SEPIC Luo converter has been particularly prominent, as mentioned in the work. Due to its low thermal conductivity, it can increase the switches' thermal utilization. By using a suitable proportional integral (PI) and artificial neural network (ANN) controller [25] technology, the bridgeless (BL) isolated PFC converter's operation is hence optimized. This technique significantly improves the converter's dynamic performance indices.

This research focuses the BL isolated SEPIC-Luo PFC as a means of improving the effectiveness of an EV battery charger. The use of the PI and ANN controller enhances the performance of the BL Isolated SEPIC-Luo PFC. The input side current and voltage distortions are decreased with the assistance of the hysteresis current controller (HCC) controller. When compared to other traditional approaches, the suggested system archives the lowest THD values.

2. PROPOSED SYSTEM DESCRIPTION

The BL isolated SEPIC-Luo converter suggested in this work is used by the efficient EV battery charger depicted in Figure 1. To control the current flowing into the EV battery while it is being charged, this adapter is built of an isolated converter. This PFC converter provides improved performance with a sizable and constant voltage gain.

In this work, a PI and ANN controller control approach is used to regulate the output from the PFC converter. A PI and ANN controller block is then given the determined error after the output voltage of the BL isolated SEPIC-Luo PFC is compared to the required reference voltage. The ANN controller outperforms the PI controller in this case in terms of delivering superior control outputs. An HCC is employed in addition to the PI and ANN controllers to improve the input side power quality. The HCC performs error correction by comparing the reference current to the input current from the AC supply. The pulse width modulation PWM generator generates pulses for the BL isolated SEPIC-Luo converter's switches based on the output from the HCC.

In this work, a PI and ANN controller control approach is used to regulate the output from the PFC converter. A PI and ANN controller block is then given the determined error after the output voltage of the BL isolated SEPIC-Luo PFC is compared to the required reference voltage. The ANN controller outperforms the PI controller in this case in terms of delivering superior control outputs. An HCC is employed in addition to the PI and ANN controllers to improve the input side power quality. The HCC performs error correction by

comparing the reference current to the input current from the AC supply. Based on the output from the HCC, the PWM generator provides pulses for the switches of the BL isolated SEPIC-Luo converter.
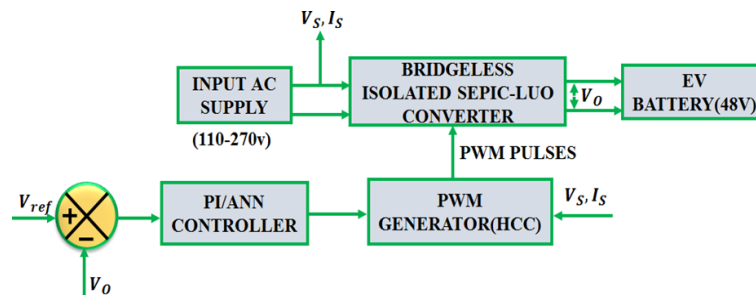
Figure 1. Schematic representation of the suggested system

3. PROPOSED SYSTEM MODELING

3.1. Modelling of BL isolated SEPIC-Luo converter

Figure 2 depicts the setup of different modes of operation of BL isolated SEPIC-Luo converter for an enhanced method-based battery charger. The BL isolated converter's functioning in the interrupted mode of operation is guaranteed to deliver a unity power factor that maintains the necessary constant level over a range of supply voltages. This design is developed by combining independent SEPIC and Luo converters that operate in two different half line. The switch of semiconductor S_1 and magnetizing transformer inductance L_{m1}, diode output D_1 and capacitor C_1 conduct in positive half cycle while Luo converter operation mode. But, the switch S_2, magnetizing inductance L_{m2} and diode output D_1 and capacitor C_2 help the SEPIC converter operate on the negative half line.

Following is an explanation of the statistical evaluation of a suggested BL isolated converter throughout the stable operation. Figure 2(a) shows the complete diagram for varies modes of operation. It is accomplished by the construction of this BL isolated converter in discontinuous conduction mode DCM that at the conclusion of every switching cycle, current via transformer's magnetizing inductance, $L_{m1,2}$ becomes discontinuous. The recommended isolated converters are presented with three alternative operating modes and associated critical actions in the Luo and SEPIC modes during the course of two different half cycles, respectively.

- Phase 1 $[\boldsymbol{t_o} - \boldsymbol{t_1}]$: The switch S_1 becomes turned on while this mode of operation. When power of the supply is stored, amount of current flowing via the input inductances L_1 and L_2 increases gradually. As seen in Figure 2(b), the voltage that flows over the energy transfer capacitor C_1, begins to decrease as the current in the inductor $Lm1$ increases. At this period, the diode D_1 fails to continue conducting.
- Phase 2 $[\boldsymbol{t_1} - \boldsymbol{t_2}]$: If switch S_1 is set to off at instant $t1$, as shown in Figure 2(c), this condition begins. D_1, the output diode, starts the process. L_{m1} begins to act as a magnet. Along the secondary side of the transformer, the energy that has been stored is discharged via the capacitor C_1, to the diode D_1 and the current through the inductor drops at an identical sloping as seen in phase-1.
- Phase 3 $[\boldsymbol{t_2} - \boldsymbol{t_3}]$: Switch S_1 stays OFF at this time. Since there is no diode current in the system, the current in the magnetizing inductance, L_{m1} is reduced. The necessary power from the battery is provided by the capacitor C_{dc}. The released energy through C_{dc} output capacitor and D_1 is turned off is displayed in Figure 2(d). According to Figures 2(e)–2(g), the aforementioned series of processes are observed in the SEPIC phase throughout the other half cycle of line voltage.
- Phase 4 $[\boldsymbol{t_3} - \boldsymbol{t_4}]$: The switch S_1 is turned on in this operational state. As the power of the supply is maintained, a steady increase in the amount of current flowing through input inductances L_1 and L_2 is observed. The current in the inductor L_{m2} expands, as seen in Figure 2(e).
- Phase 5 $[\boldsymbol{t_4} - \boldsymbol{t_5}]$: In this particular state of operation, the switch S_2 is activated. The amount of current flowing through the input inductances L_1 and L_2 is gradually increasing as the power of the electricity source remains stored. As can be seen in Figure 2(f), as current in the inductor L_{m2} expands, voltage that flows over the energy transfer capacitor C_2 starts to fall. The diode D_1 ceases operation at this point and stops conducting. Phase 6 $[\boldsymbol{t_5} - \boldsymbol{t_0}]$: In this state of operation, the switch S_1 is activated. Amount of current flowing through the input inductances L_1 and L_2 steadily increases as the power of the supply is preserved. The current in the inductor L_{m2} expands, as seen in Figure 2(g). The incorporation of an ANN controller enhances the converter's flexibility characteristics significantly. The PI controller is used for contrasting the ANN controller's operation which is explained briefly fourth coming section.
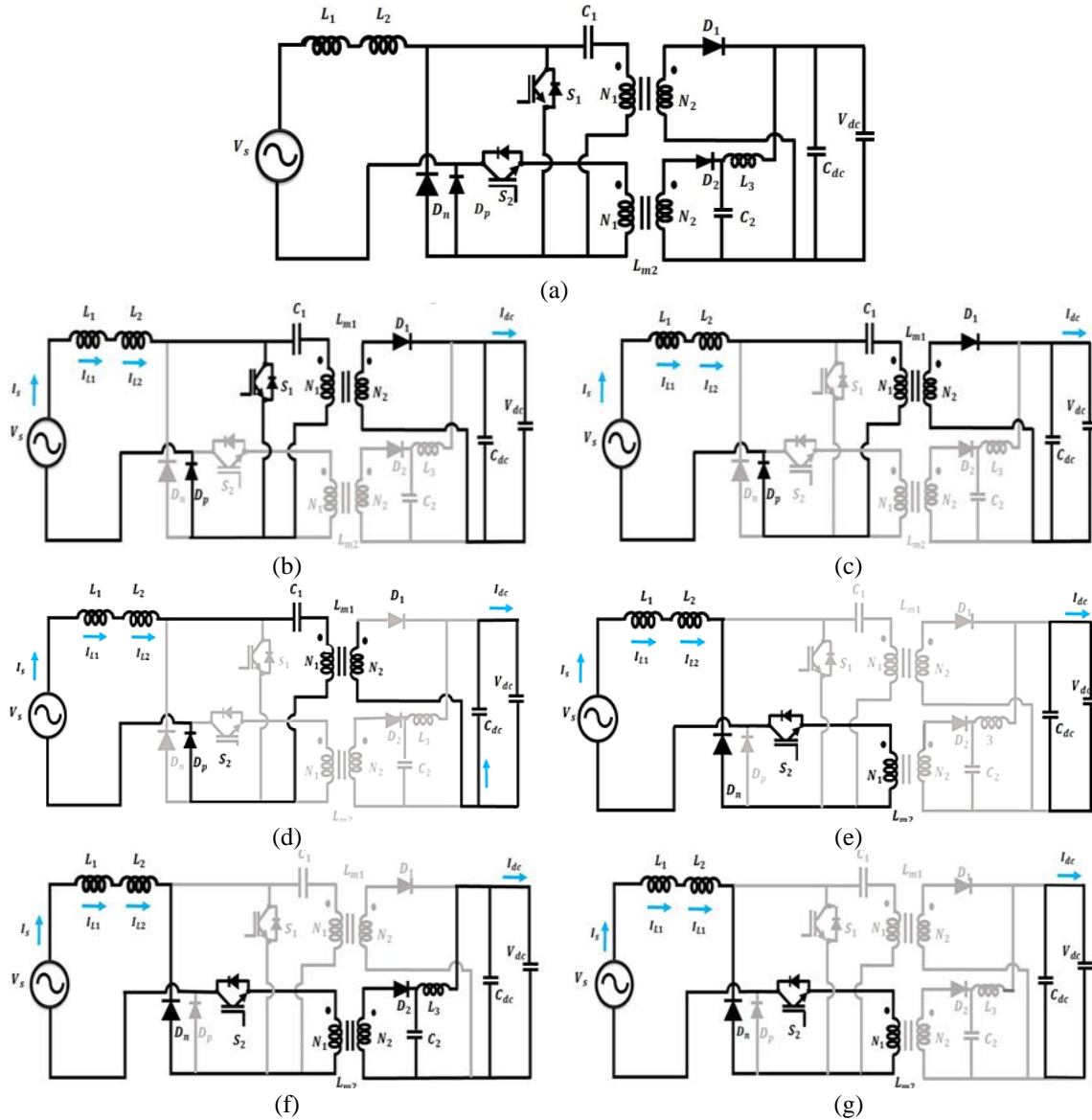
Figure 2. Mode operation of (a) proposed BL isolated SEPIC–Luo converter, (b) Phase 1 $(t_0 - t_1)$, (c) Phase 2 $(t_1 - t_2)$, (d) Phase 3 $(t_2 - t_3)$, (e) Phase 4 $(t_3 - t_4)$, (f) Phase 5 $(t_4 - t_5)$, and (g) Phase 6 $(t_5 - t_0)$

3.2. PI and ANN for control of DC link voltage
3.2.1. PI controller for DC link voltage control

One of the controllers that can be used most frequently in various sectors is the PI controller. The fundamental requirement for employing these devices is to adjust their variables to achieve the desired outcome. Different control techniques are used in relation to DC-link voltage controller. Most popular ones have a standard PI controller as their framework and have consistent proportional and integral gains.

Where, I_{gm}^{*mean} indicates the reference grid magnitude current, I_{dc}^{*mean} mean value of DC link current and $Imean$ represents the input current to DC link voltage. Figure 3 displays the mathematical expression for compressed model. The robustness of DC-link voltage control loop is guaranteed when ($K_p > 0$ and $K_i > 0$) and the minimizing of DC-link voltage variations should be considered when adjusting the K_p and K_i gains. However, the PI controller is less sufficient to resolve severe or sustained interruptions to system operation. In this work, parameter value of PI controller is $K_p = 0.1$ and $K_i = 0.01$. In addition, ANN controller is implemented to overcome the above-mentioned issue, which is briefly explained in the forthcoming section.
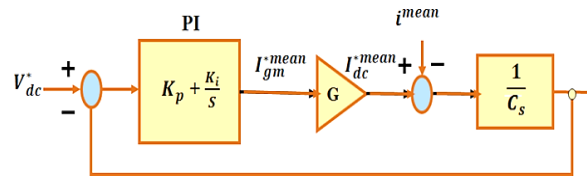
Figure 3. PI controller for DC link voltage control

3.2.2. ANN controller for DC link voltage control

An ANN is often a structure with multiple hidden layers and neurons inside each layer. Here is a conclusion: An ANN's response is comparable to real neural networks. Systematic research is done on the FF-ANN, commonly known as the feed-forward ANN. Only the forward stream of information is advanced in FF-ANN. The mathematical formula for a single neuron's output is (1).

$$y = Act(b + \sum_{i=1}^{M} x_i w_i) \tag{1}$$

While w_i, b and M denoted as activation function and input features are indicated as $x = \{x_1, x_2, x_m\}$ and each input weight is noted that x_i. An FF-ANN layer can be developed by merging various neurons into a single layer. The basic formula for the single-output and FF-ANN's is in (2) and (3).

$$y_1 = Act\left(\sum_{j=1} 2_{wj1} h_j + 2_{b1}\right) \tag{2}$$

$$h_j = Act\left(\sum_{m=1}^{M} 1_{wmj} xm + 1_{bj}\right), \forall_j = \{1, j\} \tag{3}$$

Here, the output and hidden layer indicated by ANN, (1_{wmj}, 2_{wj1}) when the output is y_1, the M and J terms denote the input neuron and hidden layer number and biases layer is represented by (1_{bj}, 2_{b1}). Figure 4 depicts the proposed system's DC link voltage control scheme. The DC voltage of reference ($V_{dc\ ref}$), output voltage ($V_{dc\ out}$) and inductor current I_L employed in the present research are selected as a developed ANN-based control scheme's input features are regarded as its intended outcome or result, whereas the ideal switching state $SOpt$ is additionally taken into consideration.

The biases and weights of the ANN are adjusted during training utilizing the Bayesian regularized technique (BRT). BRT may minimize or entirely substitute the demand for time-consuming cross-validation since it is stronger than characteristic propagation mechanisms. In the present investigation, the ANN is developed with 60% of the unpredictable input data, 20% for examination and 20% for verification. The general matrix of uncertainty, shown in Figure 5, serves for assessing the trained ANN's precision. The diagonal elements of the matrix represent the accurate categorization of the information's class, whilst other entries display an erroneous categorization of the data.
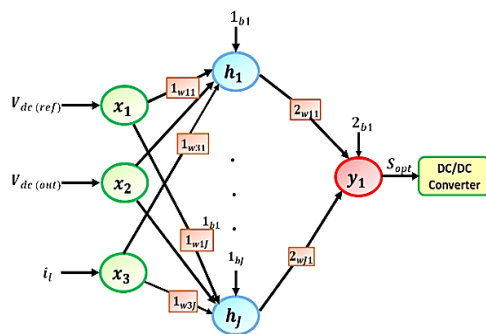

Figure 4. Control method of ANN for suggested system

Figure 5. Training matrix of ANN

It is sent to Simulink for analysis in order to determine the effectiveness of the constructed ANN model in the initial instance. Figure 6 presents the entire learning-based control method process while emphasizing the crucial elements of the training and test stages. The suggested ANN controller successfully generates the HCC reference current and maintains the stable DC link voltage.
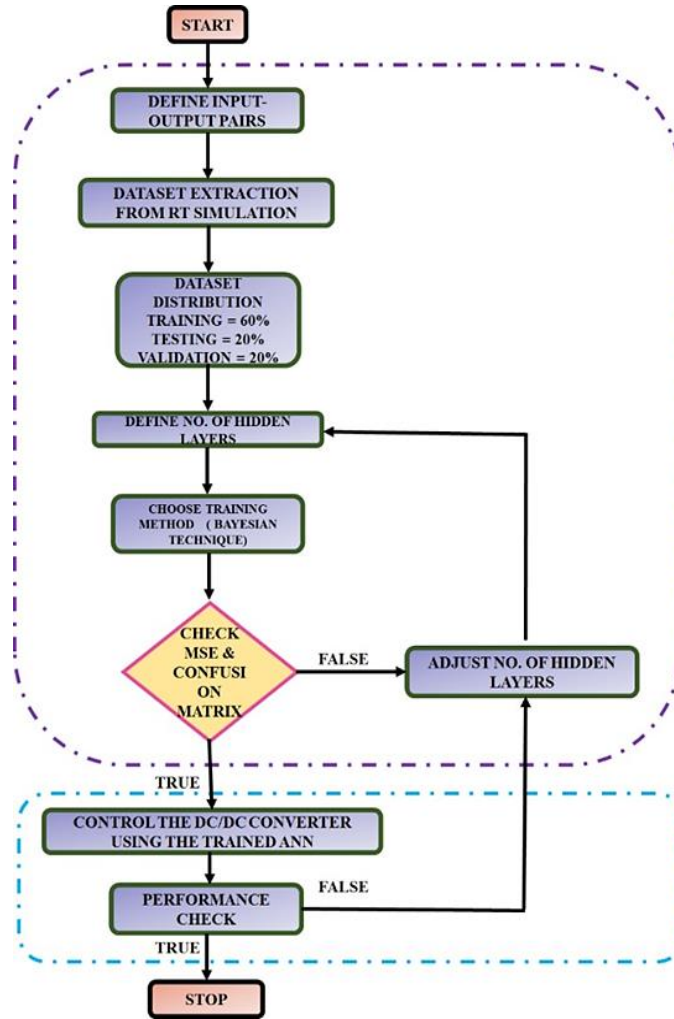
Figure 6. Flowchart for proposed control strategy

3.2.3. Modeling of HCC

Although offering many benefits, limiting cycle fluctuations, overshoot in current error, sub-harmonic production from the current and inconsistent switching represent a few disadvantages of the standard form of hysteresis controller. When using a hysteresis controller such as depicted in Figure 7, the error is transmitted instantly to the hysteresis band.
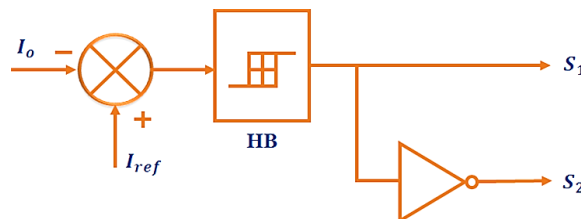

Figure 7. Flowchart for proposed control strategy

According to equation (4), the current is known as $iref$ and the difference between io and $iref$ is known as error (e). The switched behavior of a PWM generator is determined by the hysteresis band current controller.

$$e = i_o - i_{ref} \tag{4}$$

The formulation of the switching mechanism is as in (5).

$$If\ e > HB\ then\ switch\ S_1\ is\ turn\ on$$
$$If\ e > HB\ then\ switch\ S_2\ is\ turn\ on$$

$$\boldsymbol{P_L} = \frac{1}{\boldsymbol{n}} \sum_{j=1}^{n} V_s(j) V_L(j) \tag{5}$$

The reference source current is determined by (6):

$$i_{ref} = kvg \tag{6}$$

The scaling factor of k is determined by (7).

$$K = \frac{2P_L}{V_M{}^2} \tag{7}$$

The system switching frequency can be formulated by (8).

$$V_{dc} = L_f \frac{di_o}{dt} + V_g \tag{8}$$

The (9) is obtained from (4).

$$i_o = i_{re} + e \tag{9}$$

By rearranging the (8) and (9) the obtained is (10)-(13):

$$T_{ON} = 2L_f HB \frac{2L_f HB}{V_{dc} - V_g} \tag{10}$$

and,

$$T_{OFF} = 2L_f HB \frac{2L_f HB}{V_{dc} + V_g} \tag{11}$$

$$\frac{1}{f_s} = T_s = T_{ON} + T_{OFF} \tag{12}$$

$$f_s = \frac{V_{dc}{}^2 + V_g{}^2}{4V_{dc} L_f HB} \tag{13}$$

Consequently, the dc voltage, output inductance and hysteresis band significantly impact the switching frequency. As a result, the HCC eliminates input current distorted characteristics.

4.   RESULT AND DISCUSSION

The on-board EV charger is adopted in this paper to accomplish an effective PFC, with the assistance of BL-isolated SEPIC-Luo converter. A non-linear load is present, which causes distortions in the current flowing from the input supply. HCC is employed to reduce these distortions and an ANN controller is utilized to maintain a consistent output level from the converter's outputs. Using the results of MATLAB simulations, it is determined if the proposed BL isolated SEPIC PFC is effective in raising the electric power quality of the EV battery charger system. The proposed system effectively delivers constant power to the EV battery without any distortions. According to Table 1, the parameters of a proposed system include specifications for a BL isolated SEPIC-Luo converter, battery and source and output voltage.

4.1. For PI controller (230 V)

The corresponding waveforms for the input voltage $V_s = 230\ V$ and the DC resultant current 1.2 A are displayed in Figure 8. Similarly, the constant voltage of 48V is maintained. It is clear from the waveform graph that follows that the increased power factor unity technique has been successfully applied because the input current and voltage are in phase. Similarly, the SEPIC-Luo inductor current waveform appears with a maximal amplitude of 0.39 A in SEPIC mode and 5.6 A in Luo mode. The isolation transformer 1 current waveform has the greatest amplitude of 0.33 A and the transformer two waveforms have maintained the constant value of 6.8 A.

Table 1. Parameter Specification

Parameters	Value
Source voltage	180 V, 220 V, 230 V
Source current range for converter	0 – 50 A
Output DC voltage	0 – 48 V
Battery	48 A, 48 V
L_1	1.5 mH
L_2	1.5 mH
L_3	1.5 mH
C_1	1 μF
C_2	2200 μF
C_{dc}	2200 μF
Linear transformer	1:1 ratio (230 V, 50 A, 50 Hz)
L_{m1}, L_{m2}	315 mH
Switching frequency	100 kHz
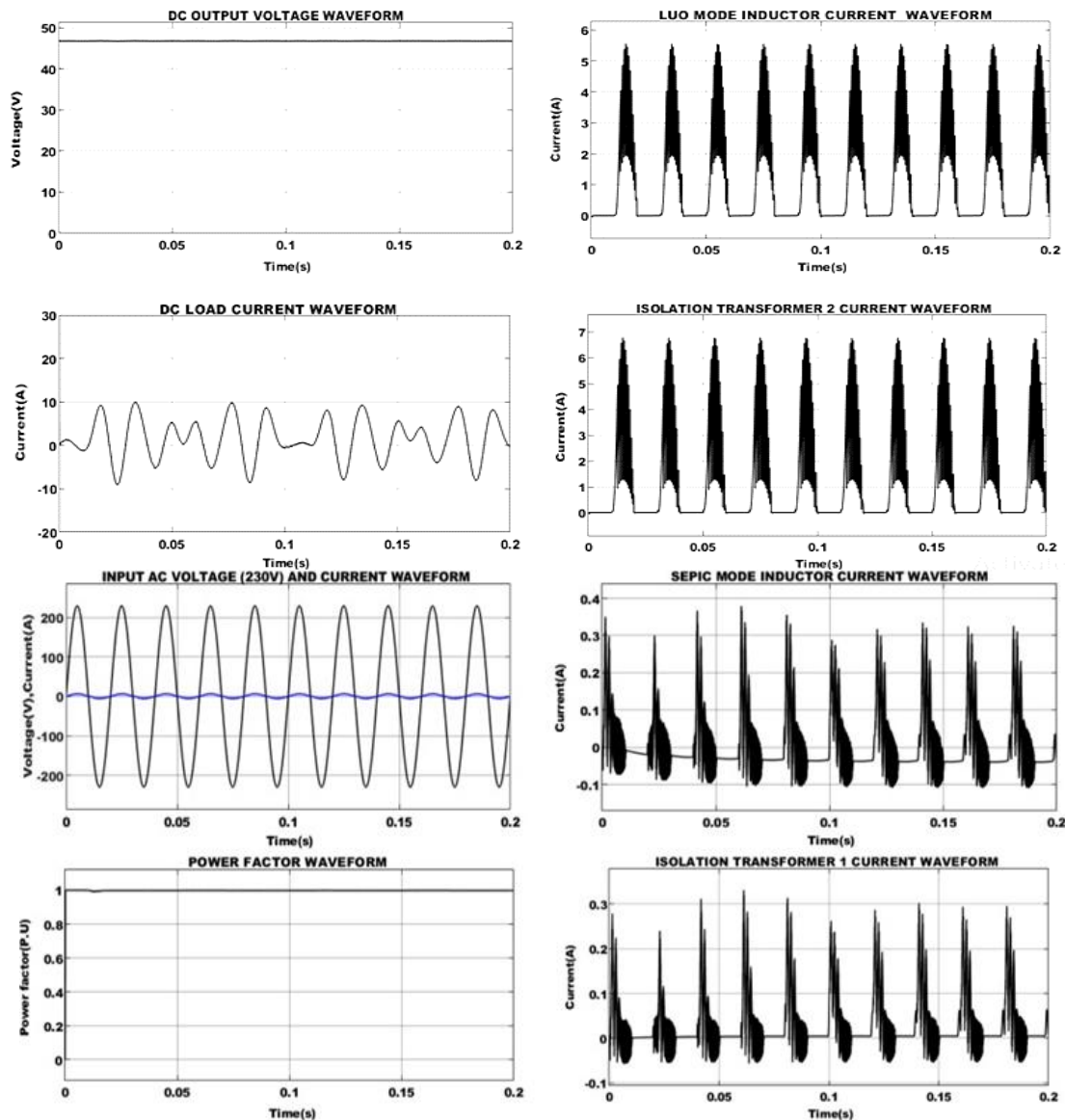
Figure 8. Waveforms of PI controller for $V_s = 230\ V$

4.2. For ANN controller (230 V)

Figure 9 shows the ANN controller with the waveforms, input voltage $Vs = 230\ V$ and DC output current 1.2 A. In the same way, the 48V constant voltage is maintained. As shown in the waveform below, the

input current and voltage have a phase that is similar, indicating that the proposed approach produced an elevated power factor. Similar in design, the SEPIC-Luo inductor current waveform has maximum amplitude of 0.38 A in SEPIC mode and 5.5 A in Luo mode. The isolation transformer 1 current waveform has the maximum amplitude value 0.33 A, while the transformer 2 current waveforms have a stable value of 6.7 A.
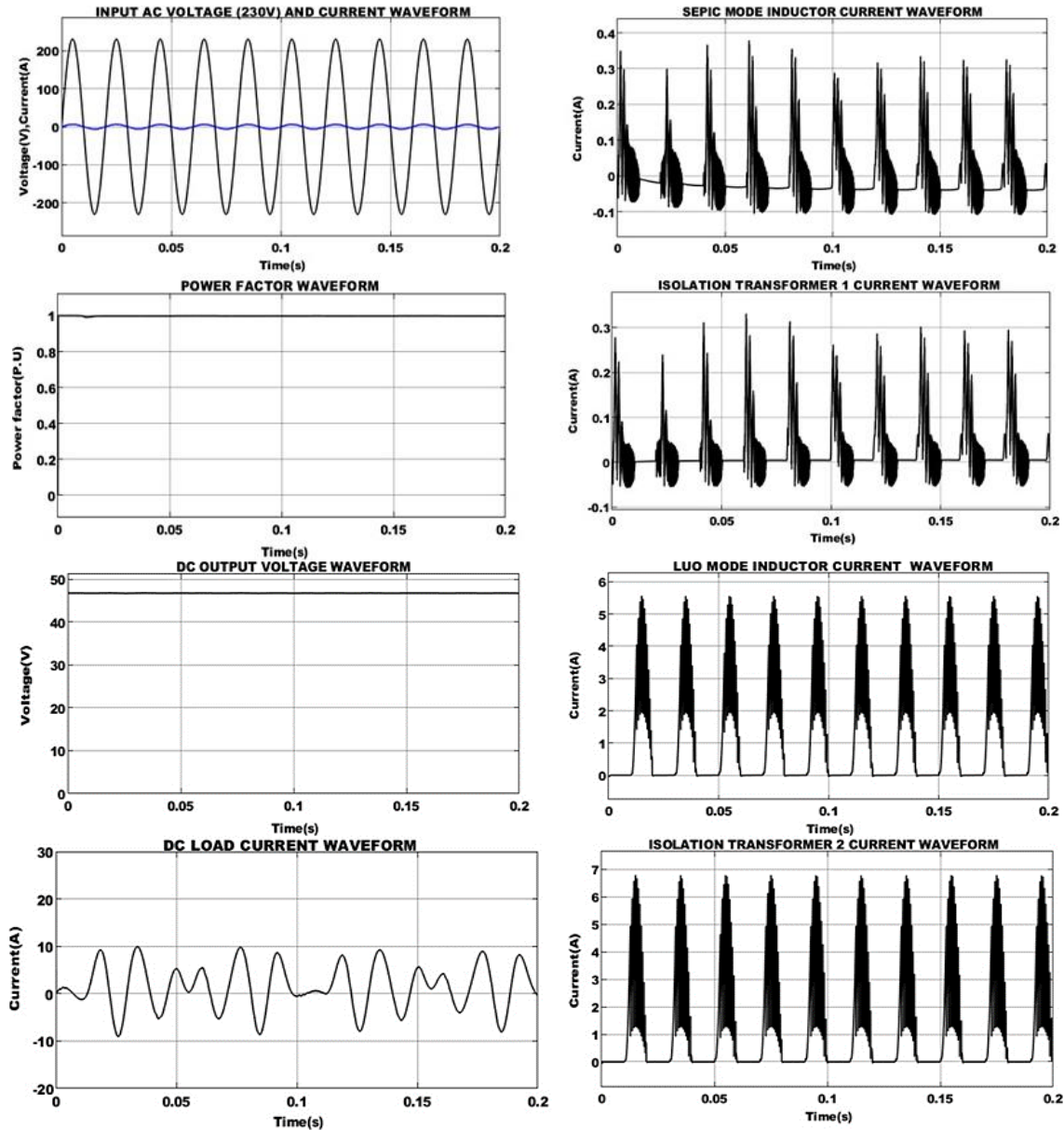
Figure 9. Waveforms of ANN controller for $V_s = 230\ V$

The resulting THD outputs of PI and ANN controller for input voltage level that is 230 V is shown in Figures 10 and 11 is respectively. Here, the THD value of PI controller is 2.95% have been achieved. Similarly, the THD output of ANN controller 1.21% is have been accomplished. The ANN controller has lowest THD values when compared to PI controller.

The suggested BL isolated SEPIC-Luo attains the maximum efficiency of 95.6% for an input supply of 180 V, which is illustrated in Figure 12. Table 2 displays the power factor values for the suggested converter as well as other common converters. For input supply of 180 V, the proposed approach generates an improved power factor output of 0.996.

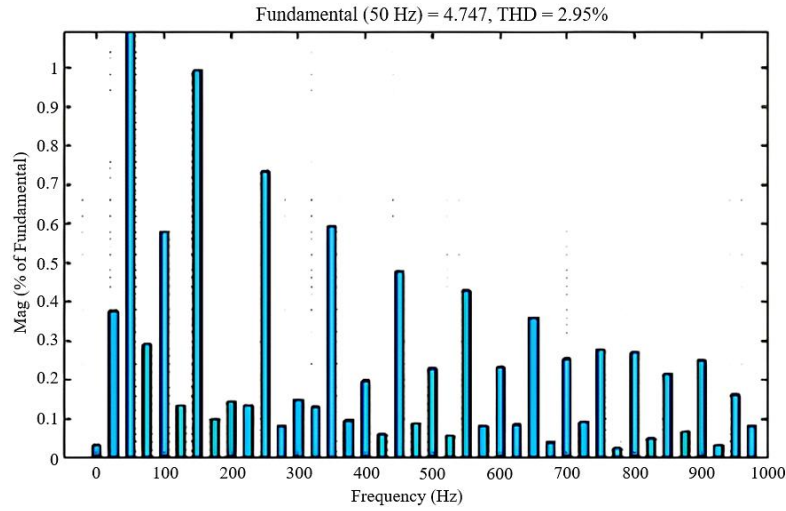$$Efficiency(\%) = \frac{OutputPower}{InputPower} = \frac{217.5*8}{180*10} = 96.5\%$$

Fundamental (50 Hz) = 4.747, THD = 2.95%

Figure 10. THD output of PI controller for input voltage 230 *V*

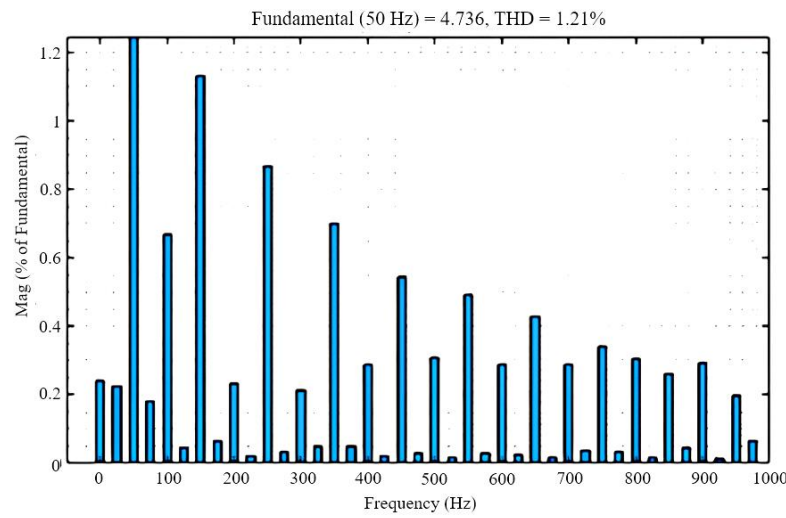Fundamental (50 Hz) = 4.736, THD = 1.21%
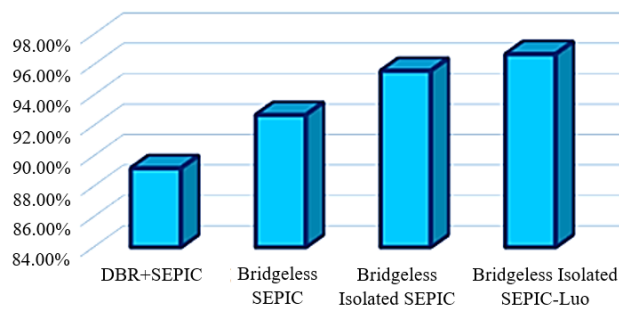
Figure 11. THD output of ANN controller for input voltage 230 *V*

Figure 12. Comparison analysis of efficiency for 180 *V*

Table 2. Comparison of power factor for 180 *V*

Converters	Power factor
DBR+SEPIC	0.899
Bridgeless SEPIC	0.989
BL isolated SEPIC	0.994
BL isolated SEPIC-Luo	0.996

5. CONCLUSION

The on-board EV charger solution suggested in this study uses a BL isolated system to maintain unity power factor and guarantee the input power quality indices. Conduction losses are significantly decreased as a result of the absence of DBR and the current conduction through a relatively few systems. The converter's performance is improved with constant DC link voltage by using an ANN and PI controller. HCC helps to reduce current distortions at the input side. With the lowest THD, the suggested converter achieves the highest efficiency of 96.7%. The attained values of THD are elaborately given below. The attained PI controller with various input ranges of THD values are 3.54% for 180 V, 3.24% for 200 V, 2.95% for 230 V and 2.81% for 270 V. Similar to this, a different voltage level is achieved with an ANN controller's THD output. The achieved THD values are 1.52% for 180 V, 1.34% for 200 V, 1.21% for 230 V and 1.04% for 270V, which are the lowest THD values when compared to PI controller. BL isolated SEPIC-Luo based PFC is used to minimize the harmonics, which lowers THD values.

REFERENCES

[1] K. S. Kavin and P. Subha Karuvelam, "PV-based Grid Interactive PMBLDC Electric Vehicle with High Gain Interleaved DC-DC SEPIC Converter," *IETE Journal of Research*, 2021, doi: 10.1080/03772063.2021.1958070.

[2] K. S. Kavin, P. Subha Karuvelam, A. Pathak, T. R. Premila, R. Hemalatha, and T. Kumar, "Modelling and Analysis of Hybrid Fuzzy Tuned PI Controller based PMBLDC Motor for Electric Vehicle Applications," *SSRG International Journal of Electrical and Electronics Engineering*, vol. 10, no. 2, pp. 8–18, 2023, doi: 10.14445/23488379/IJEEE-V10I2P102.

[3] B. Singh and R. Kushwaha, "EV battery charger with non-inverting output voltage-based bridgeless PFC Cuk converter," *IET Power Electronics*, vol. 12, no. 13, pp. 3359–3368, 2019, doi: 10.1049/iet-pel.2019.0037.

[4] A. V. J. S. Praneeth and S. S. Williamson, "A Review of Front End AC-DC Topologies in Universal Battery Charger for Electric Transportation," *2018 IEEE Transportation and Electrification Conference and Expo, ITEC 2018*, pp. 916–921, 2018, doi: 10.1109/ITEC.2018.8450186.

[5] B. Singh and R. Kushwaha, "A PFC Based EV Battery Charger Using a Bridgeless Isolated SEPIC Converter," *IEEE Transactions on Industry Applications*, vol. 56, no. 1, pp. 477–487, 2020, doi: 10.1109/TIA.2019.2951510.

[6] P. Papamanolis, D. Bortis, F. Krismer, D. Menzi, and J. W. Kolar, "New EV battery charger PFC rectifier front-end allowing full power delivery in 3-phase and 1-phase operation," *Electronics (Switzerland)*, vol. 10, no. 17, 2021, doi: 10.3390/electronics10172069.

[7] L. Kunjuramakurup, S. M. Sulthan, M. S. Ponparakkal, V. Raj, and M. Sathyajith, "A High-Power Solar PV-fed TISO DC-DC Converter for Electric Vehicle Charging Applications," *Energies*, vol. 16, no. 5, 2023, doi: 10.3390/en16052186.

[8] S. R. Meher, S. Banerjee, B. T. Vankayalapati, and R. K. Singh, "A Reconfigurable On-Board Power Converter for Electric Vehicle with Reduced Switch Count," *IEEE Transactions on Vehicular Technology*, vol. 69, no. 4, pp. 3760–3772, 2020, doi: 10.1109/TVT.2020.2973316.

[9] S. S. Indalkar and A. Sabnis, "An off Board Electric Vehicle Charger Based on ZVS Interleaved AC-DC Boost PFC Converter," *2019 8th International Conference on Power Systems: Transition towards Sustainable, Smart and Flexible Grids, ICPS 2019*, 2019, doi: 10.1109/ICPS48983.2019.9067544.

[10] A. Ali, J. Chuanwen, Z. Yan, S. Habib, and M. M. Khan, "An efficient soft-switched vienna rectifier topology for EV battery chargers," *Energy Reports*, vol. 7, pp. 5059–5073, 2021, doi: 10.1016/j.egyr.2021.08.105.

[11] J. A. Anderson, M. Haider, D. Bortis, J. W. Kolar, M. Kasper, and G. Deboy, "New synergetic control of a 20kw isolated vienna rectifier front-end ev battery charger," *2019 IEEE 20th Workshop on Control and Modeling for Power Electronics, COMPEL 2019*, 2019, doi: 10.1109/COMPEL.2019.8769657.

[12] B. Singh and R. Kushwaha, "Power Factor Preregulation in Interleaved Luo Converter-Fed Electric Vehicle Battery Charger," *IEEE Transactions on Industry Applications*, vol. 57, no. 3, pp. 2870–2882, May 2021, doi: 10.1109/TIA.2021.3061964.

[13] A. V. J. S. Praneeth and S. S. Williamson, "A wide input and output voltage range battery charger using buck-boost power factor correction converter," *Conference Proceedings - IEEE Applied Power Electronics Conference and Exposition - APEC*, vol. 2019-March, pp. 2974–2979, 2019, doi: 10.1109/APEC.2019.8721797.

[14] O. Turksoy, U. Yilmaz, and A. Teke, "Minimizing capacitance value of interleaved power factor corrected boost converter for battery charger in electric vehicles," *Elektronika ir Elektrotechnika*, vol. 25, no. 5, pp. 11–17, 2019, doi: 10.5755/j01.eie.25.5.24349.

[15] D. Menzi, D. Bortis, and J. W. Kolar, "Three-Phase Two-Phase-Clamped Boost-Buck Unity Power Factor Rectifier Employing Novel Variable DC Link Voltage Input Current Control," *Proceedings - 2018 IEEE International Power Electronics and Application Conference and Exposition, PEAC 2018*, 2018, doi: 10.1109/PEAC.2018.8590599.

[16] E. Hoevenaars, Q. Wang, P. Schumann, and M. Hiller, "Novel integrated charger concepts using six phase electrical machines as boost-buck converter," *PCIM Europe Conference Proceedings*, vol. 1, pp. 1718–1725, 2020.

[17] D. Menzi, D. Bortis, and J. W. Kolar, "A New Bidirectional Three-Phase Phase-Modular Boost-Buck AC/DC Converter," *Proceedings - 2018 IEEE International Power Electronics and Application Conference and Exposition, PEAC 2018*, 2018, doi: 10.1109/PEAC.2018.8590670.

[18] R. Kushwaha and B. Singh, "Interleaved Landsman Converter Fed EV Battery Charger with Power Factor Correction," *IEEE Transactions on Industry Applications*, pp. 1–1, 2020, doi: 10.1109/TIA.2020.2988174.

[19] R. Kushwaha and B. Singh, "An Improved SEPIC PFC Converter for Electric Vehicle Battery Charger," *2019 IEEE Industry Applications Society Annual Meeting, IAS 2019*, 2019, doi: 10.1109/IAS.2019.8912344.

[20] A. Bouafassa, L. M. Fernández-Ramírez, and B. Babes, "Power quality improvements of arc welding power supplies by modified bridgeless SEPIC PFC converter," *Journal of Power Electronics*, vol. 20, no. 6, pp. 1445–1455, 2020, doi: 10.1007/s43236-020-00143-2.

[21] B. R. Ananthapadmanabha, R. Maurya, and S. R. Arya, "Improved Power Quality Switched Inductor Cuk Converter for Battery Charging Applications," *IEEE Transactions on Power Electronics*, vol. 33, no. 11, pp. 9412–9423, 2018, doi: 10.1109/TPEL.2018.2797005.

[22] S. Dutta, S. Gangavarapu, A. K. Rathore, R. K. Singh, S. K. Mishra, and V. Khadkikar, "Novel Single-Phase Cuk-Derived Bridgeless PFC Converter for On-Board EV Charger with Reduced Number of Components," *IEEE Transactions on Industry Applications*, vol. 58, no. 3, pp. 3999–4010, 2022, doi: 10.1109/TIA.2022.3148969.

[23] C. Chaudhary, S. Mishra, and U. Nangia, "A Modified-Zeta Converter based Onboard Battery Charging with Improved THD," *Proceedings of the 8th International Conference on Signal Processing and Integrated Networks, SPIN 2021*, pp. 714–719, 2021, doi: 10.1109/SPIN52536.2021.9566059.

[24] R. Kushwaha and B. Singh, "Design and Development of Modified BL Luo Converter for PQ Improvement in EV Charger," *IEEE Transactions on Industry Applications*, pp. 1–1, 2020, doi: 10.1109/TIA.2020.2988197.

[25] E. Bas, E. Egrioglu, and T. Cansu, "Robust training of median dendritic artificial neural networks for time series forecasting," *Expert Systems with Applications*, vol. 238, p. 122080, Mar. 2024, doi: 10.1016/j.eswa.2023.122080.

BIOGRAPHIES OF AUTHORS

Meena Dhandapani received the B. Tech. degree in Electrical and Electronics Engineering from Annamalai University in 2007 and the M.E. degree in power electronics and drives from Anna University in 2010 and currently pursuing Ph.D. in the area of design of DC-DC converter for EV battery charging system from Annamalai University. Her areas of interest include the field of Power converters, application of optimization in power electronics, electrical vehicle battery charging system. She can be contacted at email: meenadhandapani86@gmail.com.

Padmathilagam Ravichandran received the B. Tech degree in Electrical and Electronics Engineering from Annamalai University in 1993 and the M.E. degree in power systems from Annamalai University in 2005 and completed her Ph.D. at Annamalai University in 2012. She is presently working as associate professor in the Department of Electrical and Electronics Engineering in Annamalai University. Her areas of interest include the field of power converters, multilevel inverter, and electrical vehicle battery charging system. She can be contacted at email: vpt_au@yahoo.co.in.

Arulvizhi Shanmugam received the B. Tech. degree in Electrical and Electronics Engineering from Annamalai University in 2001 and the M.E. degree in power systems from Annamalai University in 2004 and completed her Ph.D. at Annamalai University in 2017. She is presently working as professor in the Department of Electrical and Electronics Engineering in CK college of Engineering and Technology. Her areas of interest include the field of power electronics, renewable energy systems, and electrical vehicle battery charging system. She can be contacted at email: arulanandhan5@gmail.com.

Nammalvar Pachaivanan received the B.E. degree in Electrical and Electronics Engineering from Annamalai University, M.E degree in power electronics and drives from Anna University and completed his Ph.D. from Anna University. He is presently working as associate professor in the Department of Electrical and Electronics Engineering in Builders Engineering College. His areas of interest include in the field of power converters, renewable energy, optimization techniques, and power quality. He can be contacted at email: alvar1976@gmail.com, or pn.eee@builderscollege.edu.in.